ACS Applied Nano Materials 3.4 (2020): 3625-3633

DOI: https://doi.org/10.1021/acsanm.0c00335

Functionalization of Few-Layer Antimonene with Oligonucleotides for DNA Sensing

Tania García-Mendiola,[a,b,‡] Cristina Gutiérrez-Sánchez,[a,‡] Carlos Gibaja,[c] Iñigo Torres,[c] Carlos Busó-Rogero,[d] Felix Pariente,[a,b] Jesús Solera,[e] Zahra Razavifar,[f,g] Juan J. Palacios,[g,h,i] Félix Zamora,[b,c,d,h,] and Encarnación Lorenzo[a,b,d,*]*

[a]Departamento de Química Analítica. Universidad Autónoma de Madrid. Madrid, 28049, Spain; [b]Institute for Advanced Research in Chemical Sciences (IAdChem), Universidad Autónoma de Madrid, Ciudad Universitaria de Cantoblanco, Madrid, 28049, Spain; [c]Departamento de Química Inorgánica. Universidad Autónoma de Madrid. Madrid, 28049, Spain; [d]IMDEA Nanociencia, Ciudad Universitaria de Cantoblanco, Madrid, 28049, Spain; [e]Molecular Oncogenetics Unit. La Paz Universitary Hospital. Biochemistry

Department. Faculty of Medicine. Universidad Autónoma de Madrid. Madrid, 28046, Spain; [f]*Department of Physics, Payame Noor University, P.O. Box 19395-3697 Tehran, Iran;* [g]*Departamento de Física de la Materia Condensada, Universidad Autónoma de Madrid, Madrid, 28049, Spain;* [h]*Condensed Matter Physics Institute (IFIMAC), Universidad Autónoma de Madrid, Madrid, 28049, Spain;* [i]*Instituto Nicolás Cabrera (INC), Universidad Autónoma de Madrid, Madrid, 28049, Spain*

KEYWORDS: Antimonene, Supramolecular interactions, DNA recognition, Biosensor, Genetic diseases.

ABSTRACT: Antimonene, a novel group 15 two-dimensional material, is functionalized with an oligonucleotide as a first step to DNA sensors development. The functionalization process leads to few layers antimonene modified with DNA that after deposition on screen-printed gold electrodes gives a simple and efficient DNA electrochemical sensing platform. We provide theoretical and experimental data of the DNA-antimonene interaction confirming that oligonucleotides interact non-covalently, but strongly with antimonene. The potential utility of this antimonene-based sensing device is assessed

using, a case of study, a sequence from the gen BRCA1 as target DNA. The selectivity of the device allows not only the recognition of a specific DNA sequence, but also the detection of a mutation in this gene associated to breast cancer, directly in clinical samples.

Introduction

Two-dimensional (2D) layered materials have been recently evaluated for potential applications in optoelectronics, energy storage, environmental treatment and biomedical.[1, 2] Antimonene is one of the more recently incorporated 2D materials family members and one of the few of the so-called Xene subfamily, formed just by elements able to be isolated as 2D single layers as graphene or phosphorene.[3, 4] Despite this is a rather new material, single and few-layer antimonene, from now named as FL-antimonene, are materials stable under ambient conditions with very interesting physical and chemical properties,[5, 6] therefore, suggesting potential for interesting applications. Additionally, a large amount of physical properties has been theoretically predicted but still remains pending to be experimentally proved.[7] Very recently, the non-covalent

functionalization of the FL-antimonene has been reported with a number of organic electron-accepting molecules.[8] This reversible chemical functionalization produces an electro donor-acceptor interaction that causes modification of the physico-chemical properties of the antimonene including molecular recognition and band gap modulation.[9] Therefore, this modified material opens a wide range of new applications. However, modification with biomolecules are not much explored and scientific reports of their potential applications are currently limited, particularly in the field of biosensing.

The recent advances in the development of ultrasensitive 2D-materials based sensors for biomedical applications[10-12] have focused on graphene,[13] transition-metal dichalcogenides[14] and black phosphorus (BP),[15] showing promising results in this field. Very recently, BP has attracted attention due to its outstanding physicochemical properties.[16]

However, the poor stability of BP under ambient conditions paved the way to other 2D materials with a similar structure like group-15, also known as pnictogens.[7] Currently, antimonene has emerged as a very promising 2D material.[17] Therefore, we believe that

it is necessary to continue exploring the utility of this new nanomaterial based on its interactions with chemical and biological components.

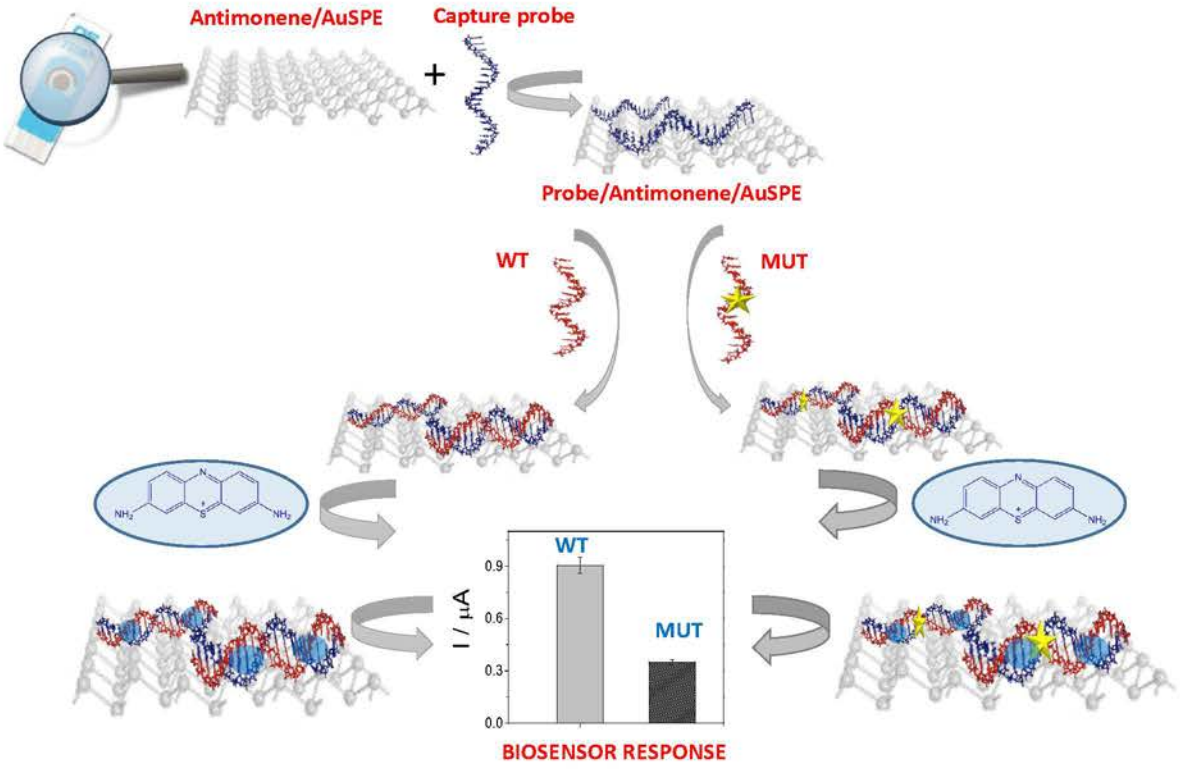

Scheme 1. Scheme of the supramolecular functionalization of antimonene with oligonucleotides and the developed DNA biosensor.

Thus, in the present work, we have studied the functionalization of FL-antimonene with a biological material, in particular, single-stranded DNA and the molecular recognition of the resulting functionalized material. Finally, as a proof-of-concept we have employed the oligonucleotide functionalized FL-antimonene to develop an efficient DNA sensor (Scheme 1) able to detect not only a specific DNA sequence, but also gene mutations associated to diseases as cancer directly in clinical samples from disease and healthy patients, the last used as control.

Nowadays the usual way to detect mutations is DNA sequencing using the classic Sanger methods. However, these methods have serious drawbacks as routine diagnosis tools, because of their laborious work and cost. Hence, the development of rapid assays, as the DNA biosensor proposed in this work, for the recognition of specific DNA sequences or the presence of DNA alterations, will result in simpler protocols and shorter time test.

Although there are some few works in the literature aiming to detect DNA alterations or single nucleotide polymorphisms (SNPs) using fluorescent microscopy or fluorescence

resonance energy transfer (FRET),[18-21] and some others based on the use of nanomaterials for biomedical applications as for example photothermal cancer therapy,[22-24] as far as we know, this is the first time that the functionalization of FL-antimonene with oligonucleotide are employed to develop a very selective DNA sensor without the need of employing chemically modified oligonucleotides.

Results and Discussion

Preparation and characterization of antimonene suspensions. FL-antimonene suspensions have been prepared by exfoliation of antimony crystals using sonication in 2-propanol. This procedure has been modified to those previously reported in the literature,[6, 8, 25] using the pure organic solvent to avoid the presence of water in the so-formed suspension and facilitate its deposition on the gold electrode avoiding coffee-ring formation.

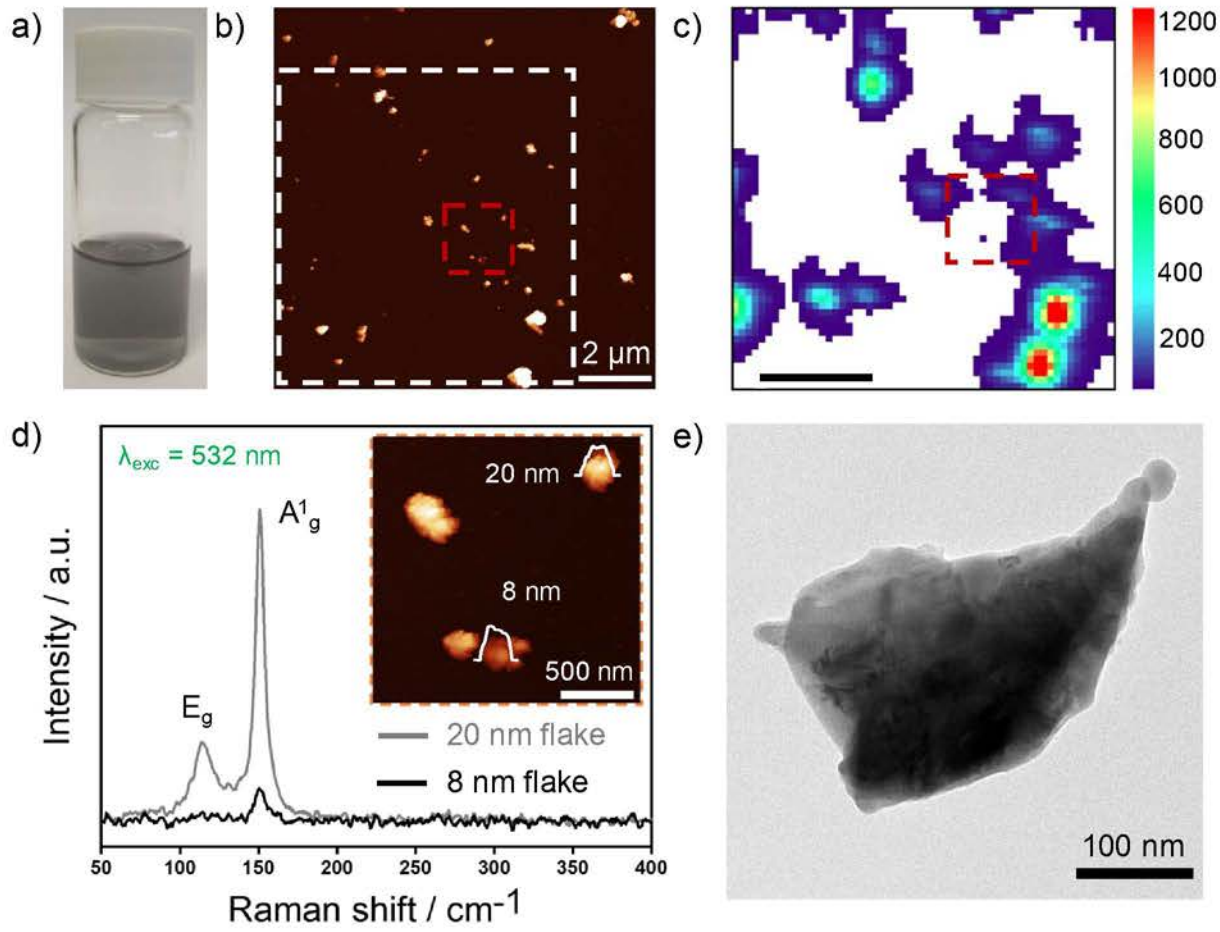

Figure 1. a) Photography of a FL-antimonene suspension in 2-propanol. b) Topographic AFM image of the 2-propanol FL-antimonene suspension drop-casted on SiO_2. c) Raman A_{1g} mapping of the FL-antimonene flakes of the area dotted in white in (b) (>14000 single point spectra over a surface area of 8 μm^2 using a step size of 200 nm), Scale bar is to 2 µm. d) Single-point spectra measured at different thicknesses according to the AFM image (inset) of the small area dotted in red in (b) and (c) showing the height profiles of

ca. 8 and 20 nm, respectively. e) TEM image of FL-antimonene flakes isolated from the suspension in (a).

Additionally, increasing the sonication time we have achieved an enhancement of the final concentration and the homogeneity of the FL-antimonene suspension. After centrifugation, the concentration of the suspension so-formed was ~ 0.2 g L^{-1} (Figure 1a and S1), which is in the order of magnitude to those already reported.[6, 8, 25] AFM images of a drop-casted SiO_2 surface show (Figure 1b) a homogeneous average area of 0.039 μm^2 and an average thickness of 16.7 nm (Figure S2 and S3). TEM images confirm the morphology observed in AFM (Figure 1e and S4). To further characterize the suspensions, statistical Raman measurements (SRMs) were carried out (Figure 1c). The characteristic phonon peaks of Sb, the A_{1g} mode at 149.8 cm^{-1} and E_g mode at 110 cm^{-1}, were revealed by SRM mappings, even for the thinnest particles detected *ca.* 8 nm, with no signature of oxidation (peaks related to the formation of Sb_2O_3 or Sb_2O_5). Even though all the antimonene flakes shown in Figure 1b can be certainly associated with the A_{1g} signals from Figure 1c, the resolution of the mapping has a broadening in the signal, what

means that their size is overestimate. A phonon softening effect was observed when the sample thickness decreases from the bulk to *ca.* 8 nm, in good agreement with theoretical predictions and recent reports (Figure 1d).[5, 6, 8, 17]

Interaction of antimonene flakes with DNA. We have studied the interaction of DNA with FL-antimonene flakes and evaluated their potential application as nanosubstrates for the direct immobilization of DNA probes to develop a DNA sensing platform.

We started these studies evaluating the absorption spectra changes of a 50 μM calf thymus single stranded DNA (ssDNA) in 0.1 M phosphate buffer (PB) solution pH 7.0 in the absence and in the presence of increasing amounts of FL-antimonene. The spectrum shows the characteristic band of the DNA in the UV region at 260 nm. A significant enhance in the absorbance is observed upon addition of increasing concentrations of FL-antimonene from 0 to 0.04 g L^{-1} (Figure S5). This hyperchromic effect is indicative of an interaction between DNA and the studied nanomaterial.[26]

The absorption spectral changes observed were used to estimate the intrinsic binding constant (K_b) which gives a quantitative estimation of the interaction strength. From the plot of the [FL-

Antimonene]/ (ε_b- ε_f) *versus* [FL-antimonene] and according to the Equation 1 (see experimental section) a value of K_b 3.7 ± 0.5 x10^3 L g $^{-1}$ was obtained. This value is similar to those reported in the literature for molecules that interacts strongly with the DNA.[27, 28]

Theoretical studies of the Antimonene-DNA interactions. In order to rationalize the interactions between antimonene and the DNA strands, theoretical calculations in the framework of density functional theory have been carried out. We have used our code ANT.G, which allows for a very efficient implementation of infinite-system boundary conditions and a robust and fast convergence. The systems studied are the four DNA nucleoside monophosphate (cytidine monophosphate, thymidine monophosphate, guanosine monophosphate, and adenosine monophosphate) adsorbed on a monolayer antimonene. Unlike the study of Xue *et. al.*[9] in which they just use nucleobases and to make a closer connection to experiments, we have taken into account the phosphate ligand associated with each base (Cytidine monophosphate, Thymidine monophosphate, Guanosine monophosphate, and Adenosine monophosphate). As expected, the presence of the phosphate group completely modifies the adsorption properties of the individual nucleobases. To begin with, the number of possible adsorption geometries is

virtually unlimited, making it very difficult to find the lowest energy one. We have explored six different possible initial orientations with respect to the substrate for each nucleoside monophosphates and let them relax to its (metastable) energy minimum. In Figure 2a we show several examples of the final configuration for each case (the other geometries considered can be found in Figure S6).

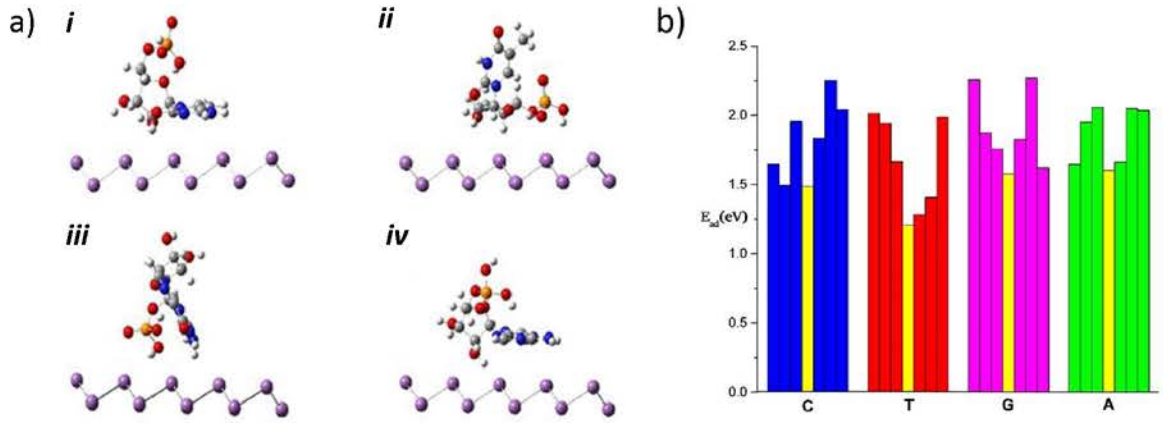

Figure 2. a) Examples of possible adsorption geometries for each DNA base+phosphate pair: *i*) Cytidine monophosphate, *ii*) Thymidine monophosphate, *iii*) Guanosine

monophosphate, and *iv*) Adenosine monophosphate. b) Adsorption energies for up to six different adsorption geometries for each nucleoside monophosphate on antimonene. Yellow bar indicates the bare base.

The adsorption energies obtained for all explored geometries are shown in Figure 2b. In yellow, we show the adsorption energy for the nucleotides, *i.e.* bare DNA bases (without the phosphate). As it can be seen, the adsorption energies considerably increase (in average) in the presence of the phosphate. Therefore, our calculations clearly support that the interaction between single stranded DNA probe, and the antimonene surface is strong[9] and it can take place using different oxygen atoms of the phosphate or sugar groups located along the DNA strand. Additionally, it suggests that, after recognition, the double stranded DNA strand will also stand on the antimonene surface because these multiple strong interaction sites. It is also worth mentioning that the in-plane antimonene nucleotides interactions are not useful to rationalize our experimental observations while

the geometry of those found via oxygen atoms of the phosphate or sugar groups are flexible to understand the interaction with a large single/double-stranded DNA strand.

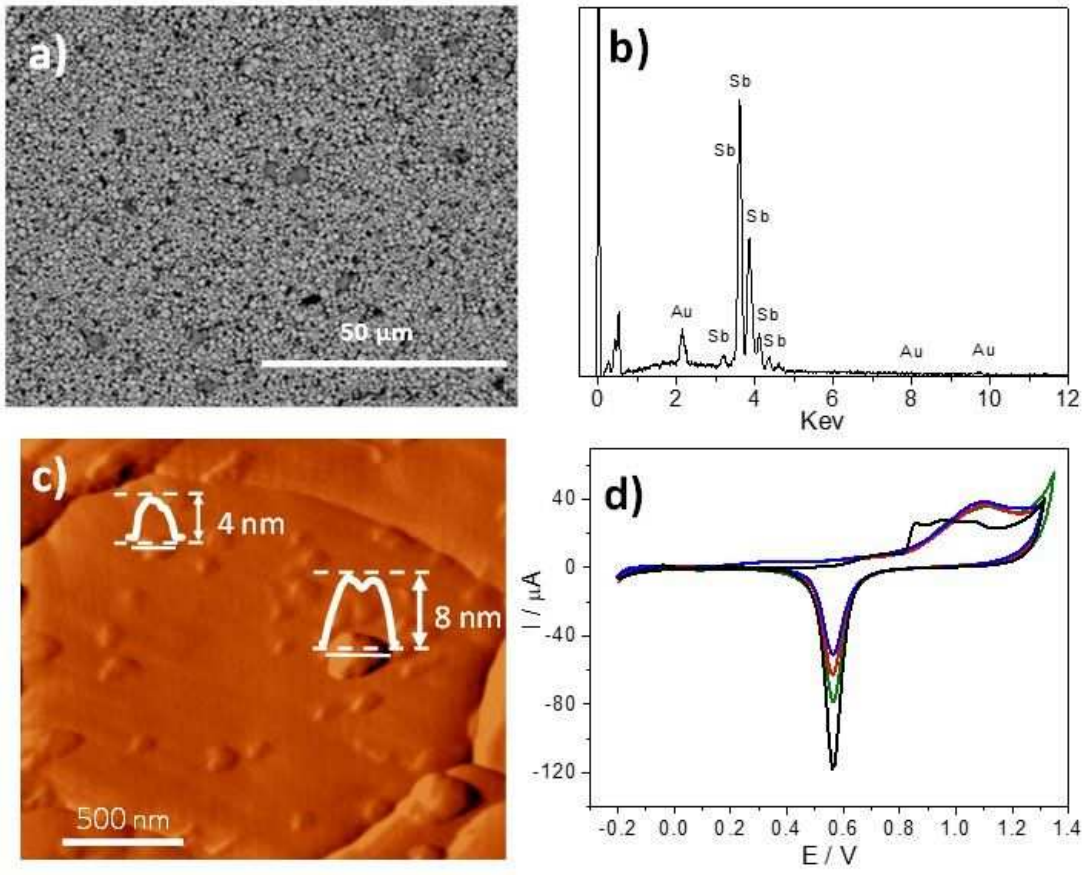

Figure 3. a) SEM images of FL-antimonene flakes deposited on AuSPE. b) EDX spectra obtained on a representative antimonene flake characterized by SEM on Figure 3a. c) Tapping mode AFM images and their height profiles of FL-antimonene on gold. d) CVs in 0.5 M H_2SO_4 at AuSPE prepared with 5 µL (green line), 10 µL (red line) and 20 µL (blue line) of a 0.2 g L^{-1} FL-antimonene suspension. Scan rate was 0.1 V s^{-1}.

DNA sensor development. Based on the above results that confirms the interaction of DNA and FL-antimonene, we have engineered a simple and efficient electrochemical platform based on the deposition of few-layer antimonene on gold screen-printed electrodes (AuSPEs) and further modification of antimonene with DNA, as base to develop a specific sensor. We fabricated and optimized the sensing system as follows: First, the antimonene modified electrode (Sb/AuSPE) was prepared by drop casting of the suspension of FL-antimonene obtained in 2-propanol on AuSPE (Figure 3). The resulting nanostructured electrode depicted in Scheme 1 was characterized by different techniques.

Figure 3a and S7b show SEM and optical images of the electrode surface, respectively. As can be seen, there is a partial cover of FL-antimonene on the Au surface, which could be noticeably identified as spots homogeneously dispersed on the Au surface when it is compared with the bare Au surface (Figure S7a and S8). EDX confirms the composition of these nanostructures (Figure 3b). Figure 3c shows a representative AFM image of FL-

antimonene flakes drop-casted onto a gold substrate, exhibiting similar features to those previously characterized on SiO_2 substrates (Figure 1b). Raman spectra of the Sb/AuSPE electrode (Figure S9) nicely correspond to FL-antimonene, *i.e.* two bands at 110 and 149 cm^{-1}, corresponding to E_g and A_{1g} similar to those depicted in Figure 1d. It indicates that FL-antimonene flakes are adsorbed on gold electrode without an additional interaction between them.

The electrochemical characterization of the Sb/AuSPE was carried out by cyclic voltammetry (CV). After the activation step, the bare AuSPE shows the characteristic CV response in 0.5 M sulfuric acid (Figure 3d). From the reduction peak of gold surface oxide, an electroactive surface area of 0.245 cm^2 is estimated (ESM). After modification with increasing amounts of FL-antimonene (5, 10 and 20 µL of a 0.2 g L^{-1} stock suspension), the CVs in 0.5 M sulfuric acid (Figure 3d) show that the process associated with the surface oxide formation of the gold microparticles is shifted to higher potentials compared with the bare AuSPE in the same conditions. This effect is concomitant with a significant decrease in the charge associated to the gold oxide reduction. In addition, double layer

region currents increase slightly due to the known enhancement of the electrochemical capacitive currents (voltammetric double layer region currents enlarged in Figure S10).[25] Thus, both decrease of the oxide reduction charge and increase of capacitive currents confirm the effective adhesion of antimonene on the AuSPE.

Based on these CV measurements, the antimonene coverage was estimated to be *ca.* 18, 36 and 46 %, for 5, 10 and 20 µL of FL-antimonene suspensions drop-casted on the electrode, respectively. The observed decrease in the electroactive area caused by the adhesion of antimonene could lead to a decrease in the conductivity of the modified electrode. Despite 20 µL of FL-antimonene provide a higher decrease in the electroactive area the stability of the Sb/AuSPE electrode is lower, for this reason 10 µL of FL-antimonene suspensions drop-casted on the electrode was used as the optimal concentration of FL-antimonene suspensions. In addition, the electrochemical behavior of the Sb/AuSPE electrode in the presence of a redox probe such as thionine was studied. The CV of thionine at a Sb/AuSPE (Figure S11, red line) in 0.1 M phosphate buffer (PB) pH 7.0 shows a redox couple at a formal potential (E°) of − 0.428 V assigned to the

oxidation/reduction of the thionine in aqueous media. The anodic to cathodic peak currents ratio (Ip_a/Ip_c) is close to unity and the peak potential separation is that expected for two-electron reversible redox process. In contrast with the electrochemical behavior observed at bare AuSPE electrode (Figure S11, black line), the current intensity is slightly enhanced as one would expect due to the increase in the effective surface area caused by the nanomaterial.

Once the Sb/AuSPE was properly characterized, its potential application as nanosubstrates for the direct immobilization of unmodified DNA probes, in order to develop an electrochemical DNA sensing platform, was evaluated. Thus, a platform for the detection of a specific sequence of gene BRCA1 as a prototype system was fabricated and optimized. This platform was selected as a prototype with the aim of developing approaches with wide applicability. Scheme 1 shows a sketch of the device. The first step for the prototype device fabrication was the immobilization of the $PROBE_{BRCA1}$, a synthetic single stranded 100-mer sequence of this gene directly by drop casting onto the

antimonene (see experimental section), based on the strong interaction of nucleobases and antimonene.[9]

The next step, after BRAC1 probe immobilization onto the antimonene-based electrochemical platform, was to text the ability of the probe modified FL-flakes to recognize the target ssDNA and mutation detection based on the hybridization event (Scheme 1). For this purpose, we employed thionine as redox indicator. In the first hybridization essay, a fully complementary synthetic sequence ($BRCA1_C$) of the probe was chosen as the objective. The hybridization and thionine accumulation steps are indicated in the experimental section. The CV behavior of thionine accumulated at a $PROBE_{BRAC1}$ Sb/AuSPE platform after hybridization with $BRCA1_C$ shows a dramatic enhancement of the current (Figure S11, blue line) compared to the response at Sb/AuSPE platform (Figure S11, red line). In addition, a more reversible redox couple system, as is demonstrated with the decrease in the ΔE_P (to values around 50 mV) is observed. These facts indicate that the thionine is collected on the double stranded DNA (dsDNA) film formed at the platform after hybridization between the probe and the target

DNA. In order to electrochemically drive this accumulation, the potential was cycled for about 100 cycles (Figure S12). The device response is based on the detection of the hybridization event between the immobilized $PROBE_{BRCA1}$ and the target sequence, which is followed by the electrolysis of the dye accumulated at the immobilized $PROBE_{BRCA1}$ before and after hybridization with the target DNA.

In order obtain a better differentiation of the thionine signal and current background, Differential Pulse Voltammetry (DPV) was employed. Thus, the response is based on changes in thionine DPV peak currents before and after hybridization.

Hybridization of the immobilized $PROBE_{BRCA1}$ with the fully complementary sequence results in a dramatic increase in the DPV thionine peak current (Figure S13, blue line) compared to the peak current obtained before hybridization (Figure S13, black line). As a control, the DPV of thionine accumulated on a platform without the DNA probe (Sb/AuSPE) has also been included. In the absence of DNA, thionine does not accumulate as it can be observed from the slight current observed (Figure S13, orange

line). These results confirm that both the hybridization event detection and the analyte sequence recognition are feasible using the antimonene-based DNA platform.

The selectivity of the device was assessed by its response to an analyte sequence containing a point mutation ($BRCA1_{SM}$) under the same hybridization conditions used for the perfect complementary sequence. It would expect that the hybridization of the DNA probe with the mutated target will lead a distortion of the DNA double-helix, which may interact with thionine in a different extension. Based on this assumption, it can be anticipated a distinct current response in comparation with those obtained with the complementary sequence. The DPV peak current of thionine demonstrates that the response to the single-mismatched target is much smaller (Figure S13, red line) than that obtained for the fully complementary sequence (Figure S13, blue line), allowing to unequivocally discriminate between both samples.

Direct detection of a specific gene mutation in clinical samples. The applicability of the device as a fast screening method of specific gene mutations was evaluated by analyzing

directly genomic DNA clinical samples extracted from human blood cells of patients carrying a mutation in gene BRCA1, without other sample treatment than dilution. We have focused on a specific mutation of the exon 9 of this gene, consisting on a change of a cytosine by a thymine. Gene sequencing is the most common technique for identifying gene mutations. Nevertheless, these methods present numerous drawbacks as usual diagnosis tools, because of their laborious work and cost. Portable devices, such as electrochemical biosensors, can be a good alternative as preliminary screening test for mutation detection associated to genetic diseases such as cancer, because they are fast and inexpensive.[29-31] As it is described in the experimental section when the device is applied for analyzing clinical samples, we follow the same strategy described above for synthetic DNA sequences and depicted in Scheme 1 but using as target DNA denatured clinical samples. The mutation detection consist on the comparison of the electrochemical response of the hybridization reaction between $PROBE_{BRCA1}$ (a synthetic single stranded DNA sequence of 100-mer complementary to the wild type analyte) and the denaturized DNA samples, which comprise around 220-mer PCR amplicons of the wild type form (WT) from healthy patients (used as control) or the mutated form (MUT) from disease patients,

who carry the mutation of BRCA1 gene (Table S1). These samples were provided and validated by sequencing in La Paz Hospital.

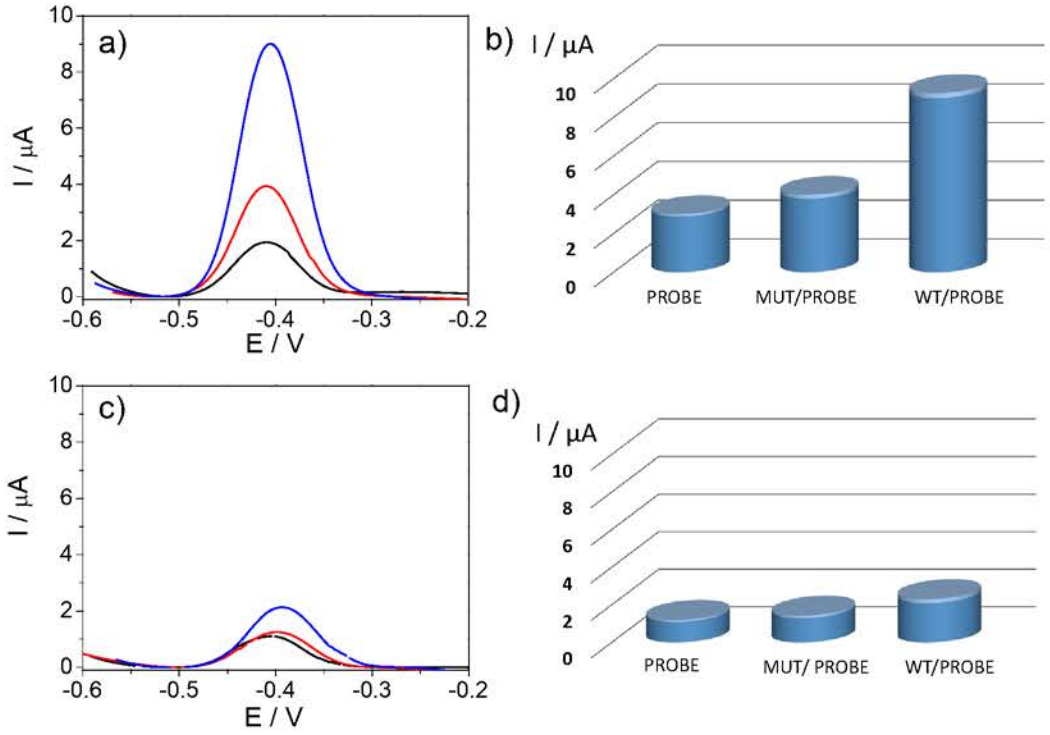

Figure 4. DPV in 0.1 M PB pH 7.0 of: a) Sb/AuSPE modified with the DNA probe; before (black line) and after hybridization with the MUT (red line) or WT (blue line) from clinical samples; c) AuSPE (without antimonene) modified with the DNA probe before (black line) and after hybridization with MUT (red line) or WT (blue line) from clinical samples; b) bar

diagrams of the direct DNA sensor response to clinical samples; d) bar diagrams of the response to clinical samples of a sensor prepared without antimonene ($PROBE_{BRCA1}$/AuSPE). Error bars in Figure 4b and 4d were calculated with the standard deviation obtained using five different biosensors (n = 5).

Figure 4a and 4b show DPVs and bar diagram, respectively, of the biosensor signal to the WT and MUT samples. They demonstrate that when the hybridization occurs with the MUT, the current intensity resulted is less than half to that observed with the WT (used as control). We also evaluated the reproducibility of the device using the signal obtained of five different biosensors (constructed identical) to either WT or MUT target DNA and was found to be of 95 % in both cases. Values of 9.0 ± 0.5 μA and 3.8 ± 0.2 μA for WT and MUT, respectively were obtained as it is depicted in the bar diagrams of Figure 4b.

Taking into account that the error obtained for all the biosensors is less than 5 %, it can be concluded that the present screening method efficiently discriminates between clinical samples from healthy (WT samples) and disease patients (MUT samples) with the only

treatment of these samples than dilution. The main role of the antimonene was also evaluated by comparison with devices prepared in the same manner but without antimonene, using a bare AuSPE (Figure 4c and 4d). As it can be observed when the hybridization event takes place with the complementary sequence no significant increase in the signal currents is detected. Hence neither the hybridization nor the mutation can be detected with devices prepared without antimonene as nanosubstrate for DNA probe immobilization.

We have also evaluated the analytical parameters of the proposed method. The electrochemical signal shows excellent correlation (Figure 5) with the amount of the target sequence (WT_{BRCA1}) up to 20.0 ng μL^{-1} and the detection limit was found to be 28.3 pg μL^{-1} (according to the $3 \times S_b . m^{-1}$ criteria, where S_b corresponds to the standard deviation (n = 5) of measurements made with the DNA probe and “m” is the slope of the calibration plot). The sensitivity of the biosensor was found to be 1.06 $\mu A/ng^{-1}$ μL^{-1}. In addition, we evaluated the stability or durability of the biosensor using different

$PROBE_{BRCA1}$/Sb/AuSPE electrodes to detect WT sequence over a period of one month giving very similar responses (98 %) and without losing the ability of detection.

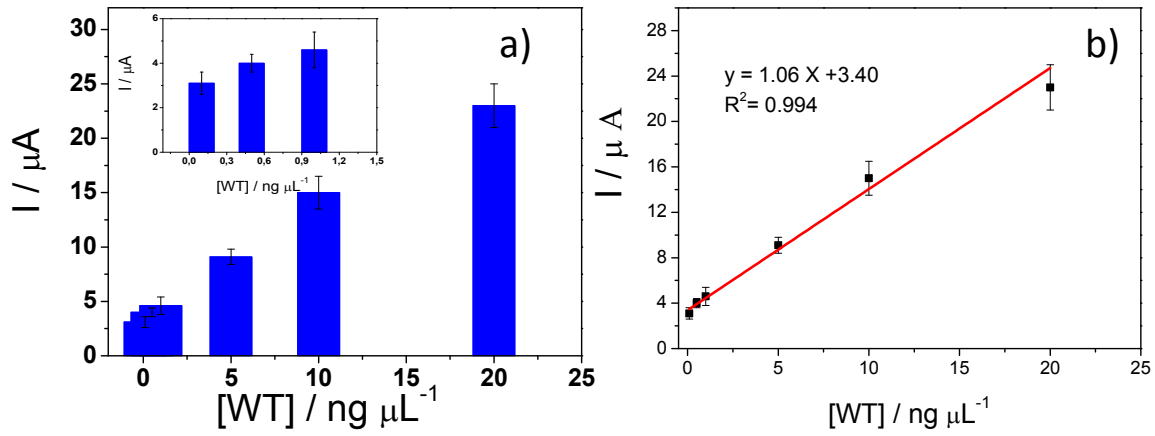

Figure 5. a) Bar diagrams of the peak current of the biosensor after hybridization with different concentrations of WT sequence (from 0.1 ng μL^{-1} to 20.0 ng μL^{-1}) after thionine accumulation by applying potential cycling. Inset: magnification of the lower concentrations 0.1, 0.5 and 1.0 ng·μL^{-1}. b) Representation of the calibration plot. The error bars were calculated using the standard deviation obtained from five different biosensors (n = 5).

Conclusions

We have carried out the supramolecular functionalization of antimonene with DNA. We have theoretically and experimentally demonstrated that antimonene interacts non-covalently, but strongly with oligonucleotides. Theoretical calculations have confirmed that after modification, single-stranded oligonucleotides adopt on antimonene layer, many different conformational configurations, allowing to hybridize them with their complementary oligonucleotide. Based on these results, as a proof-of-concept, we have developed a simple and efficient electrochemical DNA sensor based on the interaction between a single stranded oligonucleotide and few-layer antimonene deposited on gold screen-printed electrodes.

The device can be applied as a fast and accurate screening method for mutation detection in BRAC1 gene directly in clinical samples with a low detection limit, used to search for generational inheritance patterns related with specific diseases,[32] avoiding the use of previously expensive treated/modified DNA probes. Hence, a broad range of applications of this kind of sensors is expected because their preparation and utilization

protocols are not complicated, inexpensive, and fast or non-time consuming. It can be considered as new device with enormous potential for the design of point-of-care molecular diagnostic systems because of its simplicity. It represents a competitive option to the traditional and conventional gene assay.

Experimental Section

Antimony powder from Smart Elements (99.9999 % purity), 2-Propanol from Panreac > 99.8 %. Thionine, H_2SO_4 98 %, sodium phosphate dibasic ≥ 99 %, sodium phosphate monobasic monohydrate ≥ 99 % and 2-propanol were purchased from Sigma-Aldrich. Aqueous solutions were prepared using Milli Q water (18.2 MΩ·cm).

Sigma-Aldrich Co. dsDNA supplies double stranded calf thymus DNA (dsDNA). 1.0 mg mL^{-1} stock solutions of dsDNA were prepared in 0.1 M PB pH 7.0. The absorbance ratio at 260 and 280 nm of the DNA was found to be 1.9 which suggests no presence of protein.[32] Custom-made single stranded synthetic oligonucleotides, 110-mer, from sequences of BRCA1 gene ($PROBE_{BRCA1}$, $BRCA1_C$, $BRCA1_{SM}$) were purchased by

Sigma-Aldrich Co. (Table S1). Clinical DNA samples of BRCA1 gene from healthy (wild type, WT) or disease patients, who has the mutation (MUT), were supplied and checked by Hospital La Paz and are listed in Table S1.

Antimony Preparation. This procedure involves a pre-grinding process of the antimony crystals with an Agathe mortar giving rise to a so-called grinded antimony. A 20 mL ball mill reactor (IKA Ultra-Turrax Tube Drive Control) was charged with 200 mg of grinded antimony and 30 stainless steel balls, to complete a total volume of 7.5 mL. Then, the mixture stirred in the reactor for 180 min at 3000 rpm, and the resulting antimony particles were separated from the stainless-steel balls.

Ultrasonic bath assisted exfoliation process. 10 mg of dry ball-milled antimony was placed in a 20 mL vial with 10 mL of 2-Propanol. The mixture was sonicated for 120 min in the ultrasonic bath at 380 W and 37 kHz. Then, the resulting black suspension was centrifuged at 3000 rpm (845 rcf) for 1 min, in order to eliminate the unexfoliated crystals, and the clear supernatant was recovered. 20 µL of the suspension were casted on a SiO_2 surface and dried under an argon flow before drying completely. Sonication was

performed using an Elmasonic P300H ultrasonic bath. Centrifugation was carried out in an MPW-350R centrifuge using 2 mL Eppendorf.

Interaction of antimonene-DNA. UV-visible absorption spectra were performed in quartz cells using 0.1 M PB pH 7.0 as solvent. Titrations base on the UV-visible absorption spectra were obtained using 100 μM of ssDNA and varying the concentration of antimonene from 0 to 0.04 g L^{-1}. K_b or the intrinsic binding constant, , was determined using the equation reported by Meehan *et al*[34]:

$$[\text{FL antimonene}] / (\varepsilon_b - \varepsilon_f) = [\text{FL antimonene}] / (\varepsilon_a - \varepsilon_f) + 1 / K_b (\varepsilon_a - \varepsilon_f) \quad \text{Equation 1}$$

where ε_a is the molar absorptivity of ssDNA when different concentrations of antimonene are used, ε_f and ε_b are the molar absorptivity for free and bound forms of ssDNA, respectively.

K_b value was obtained from the quotient of the slop and the intercept of the plot [FL antimonene] / (ε_b- ε_f) vs [FL antimonene] (Figure S5).

Screen printed electrodes modification by antimonene suspensions. Gold screen-printed electrodes (AuSPE) were cleaned and activated by cyclic voltammetry in 0.5 M H_2SO_4, 10 cycles. Immediately, the surfaces were modified by drop casting with 10 µL of 0.2 g L^{-1} FL-antimonene suspension (Sb/AuSPE). The total electroactive surface area of AuSPE electrode was determined by the integration of the gold oxide reduction peak, taking into account a charge of −390 µC cm^{-2} for the reduction of a gold oxide monolayer.[35]

DNA extraction and purification from peripheral blood samples and PCR amplification. Genomic DNA used for the analysis was obtained from patient's peripheral blood cells using Qiagen DNA Blood kit (Qiagen Iberia, Las Rozas, Spain) and the chemagen - Perkin Elmer platform (Perkinelmer España, Madrid, Spain) according to manufacturers' instructions. Once the genomic DNA was obtained, the first step in the approach involved the analysis by PCR amplification of each canonical exon, using oligonucleotides

annealing to the flanking introns. Each amplicon was analyzed by agarose gel electrophoresis and all PCR products were sequenced by Sanger. We performed the analysis of all coding exons, in order to explore every potential mutated allele on BRCA1 gene. In addition, MLPA analysis was carried out to identify any potential genomic deletion or duplication, using MLPA kits (MRC-Holland, the Netherlands) and following manufacturers' instructions. Clinical samples were just diluted in 10 mM PB pH 7.0 + 0.4 M NaCl to a final concentration of 5.0 ng μL^{-1}.

Modification of antimonene with DNA and sensor development. Few-Layer antimonene immobilized on a gold electrode (Sb/AuSPE) was modified with 10 µL of 40 µM $PROBE_{BRCA1}$ synthetic sequence solution ($PROBE_{BRCA1}$/Sb/AuSPE). Afterwards, during 24 h the electrode was kept at room temperature. Then, during 30 min it was soaked with sterile water. Before hybridization event, PCR samples were denatured. For this purpose, they were heated at 100 ºC during 30 min followed by quick cooling. The $PROBE_{BRCA1}$ immobilized on the gold electrode ($PROBE_{BRCA1}$/Sb/AuSPE) was hybridized for 1 h at 40 ºC with the target DNA in 10 mM PB pH 7.0 + 0.4 M NaCl. Two types of DNA were used

as target: synthetic oligonucleotides and clinical samples of gen BRCA1: 10 µL of a 20 µM fully complementary ($BRCA1_C$) or carrying a mismatch ($BRCA1_{SM}$) synthetic sequence were added to the $PROBE_{BRCA1}$ modified electrode. The resulting modified electrodes are named as $BRCA1_C/PROBE_{BRCA1}/Sb/AuSPE$ and $BRCA1_{SM}/PROBE_{BRCA1}/Sb/AuSPE$, respectively. 10 µL of a 5.0 ng μL^{-1} denatured clinical sample, consisting of a wild type (WT) or a mutated form (MUT) of BRCA1 gene were added to the $PROBE_{BRCA1}$ modified electrode. The resulting modified electrodes are named as $WT/PROBE_{BRCA1}/Sb/AuSPE$ and $MUT/PROBE_{BRCA1}/Sb/AuSPE$, respectively. Afterwards, the modified electrodes were immersed in 1.0 mM of thionine using 0.1M PB pH 7.0 as solvent. Then, and the potential was cycled at 100 mV s^{-1} for100 times. Finally, sterile water was used to rinse the electrodes and they were placed in 0.1M PB pH 7.0, subsequentially differential pulse voltammograms were immediately recorded.

Theoretical calculations. The ANT.G code is available at https://www.simuneatomistics.com. For all the calculations we have used a GGA

functional[36, 37] with semiempirical dispersion and the LanL2dZ basis set.[38] Details of the implementation in ANT.G can be found in the literature.[39, 40]

ASSOCIATED CONTENT

Supporting Information. A PDF file is available free of charge with additional experimental details of the electrochemical characterization, AFM, SEM, TEM imaging and Raman spectroscopy measurements is available.

AUTHOR INFORMATION

Corresponding Author

* Corresponding_Author: Email: felix.zamora@uam.es; encarnacion.lorenzo@uam.es.

Author Contributions

‡These authors contributed equally.

ACKNOWLEDGMENTS

Ministerio de Ciencia Innovación y Universidades (CTQ2017-84309-C2-1-R, MAT2016-77608-C3-1-P, PCI2018-093081, JTC2017/2D-Sb&Ge, FIS2016-80434-P), Generalitat

Valenciana (APOSTD/2017/010) and CAM (TransNANOAVANSENS and 2017-T1/BIO-5435) are gratefully acknowledged. We also acknowledge the María de Maeztu Programme for Units of Excellence in R\&D (MDM-2014-0377), the Fundación Ramón Areces and the computer resources and assistance provided by the Centro de Computación Científica of the Universidad Autónoma de Madrid.

REFERENCES

(1) Choi, W.; Choudhary, N.; Han, G. H.; Park, J.; Akinwande, D.; Lee, Y. H., Recent development of two-dimensional transition metal dichalcogenides and their applications. *Mater. Today* **2017,** 20, 116-130.

(2) Tan, C.; Cao, X.; Wu, X.-J.; He, Q.; Yang, J.; Zhang, X.; Chen, J.; Zhao, W.; Han, S.; Nam, G.-H.; Sindoro, M.; Zhang, H., Recent Advances in Ultrathin Two-Dimensional Nanomaterials. *Chem. Rev.* **2017,** 117, 6225-6331.

(3) Geim, A. K.; Novoselov, K. S., The rise of graphene. *Nat. Mate.r* **2007,** 6, 183-191.

(4) Castellanos-Gomez, A.; Vicarelli, L.; Prada, E.; Island, J. O.; Narasimha-Acharya, K. L.; Blanter, S. I.; Groenendijk, D. J.; Buscema, M.; Steele, G. A.; Alvarez, J. V.;

Zandbergen, H. W.; Palacios, J. J.; van der Zant, H. S. J., Isolation and characterization of few-layer black phosphorus. *2D Mater.* **2014,** 1, 025001.

(5) Ares, P.; Aguilar-Galindo, F.; Rodriguez-San-Miguel, D.; Aldave, D. A.; Diaz-Tendero, S.; Alcami, M.; Martin, F.; Gomez-Herrero, J.; Zamora, F., Mechanical Isolation of Highly Stable Antimonene under Ambient Conditions. *Adv. Mater.* **2016,** 28, 6332-6336.

(6) Gibaja, C.; Rodriguez-San-Miguel, D.; Ares, P.; Gómez-Herrero, J.; Varela, M.; Gillen, R.; Maultzsch, J.; Hauke, F.; Hirsch, A.; Abellán, G.; Zamora, F., Few-Layer Antimonene by Liquid-Phase Exfoliation. *Angew. Chem. Int. Ed.* **2016,** 55, 14345-14349.

(7) Zhang, S.; Guo, S.; Chen, Z.; Wang, Y.; Gao, H.; Gómez-Herrero, J.; Ares, P.; Zamora, F.; Zhu, Z.; Zeng, H., Recent progress in 2D group-VA semiconductors: from theory to experiment. *Chem. Soc. Rev.* **2018,** 47, 982-1021.

(8) Abellan, G.; Ares, P.; Wild, S.; Nuin, E.; Neiss, C.; Rodriguez-San Miguel, D.; Segovia, P.; Gibaja, C.; Michel, E. G.; Gorling, A.; Hauke, F.; Gomez-Herrero, J.; Hirsch, A.; Zamora, F. L., Noncovalent Functionalization and Charge Transfer in Antimonene. *Angew. Chem. Int. Ed.* **2017,** 56, 14389-14394.

(9) Xue, T.; Liang, W.; Li, Y.; Sun, Y.; Xiang, Y.; Zhang, Y.; Dai, Z.; Duo, Y.; Wu, L.; Qi, K.; Shivananju, B. N.; Zhang, L.; Cui, X.; Zhang, H.; Bao, Q., Ultrasensitive detection of miRNA with an antimonene-based surface plasmon resonance sensor. *Nat. Commun.* **2019,** 10.

(10) Chen, Y.; Tan, C.; Zhang, H.; Wang, L., Two-dimensional graphene analogues for biomedical applications. *Chem. Soc. Rev.* **2015,** 44, 2681-2701.

(11) Chimene, D.; Alge, D. L.; Gaharwar, A. K., Two-Dimensional Nanomaterials for Biomedical Applications: Emerging Trends and Future Prospects. *Adv. Mater.* **2015,** 27, 7261-7284.

(12) Kurapati, R.; Kostarelos, K.; Prato, M.; Bianco, A., Biomedical Uses for 2D Materials Beyond Graphene: Current Advances and Challenges Ahead. *Adv. Mater.* **2016,** 28, 6052-6074.

(13) Lee, J.; Kim, J.; Kim, S.; Min, D.-H., Biosensors based on graphene oxide and its biomedical application. *Adv. Drug Deliv. Rev.* **2016,** 105, 275-287.

(14) Mayorga-Martinez, C. C.; Khezri, B.; Eng, A. Y. S.; Sofer, Z.; Ulbrich, P.; Pumera, M., Bipolar Electrochemical Synthesis of WS2 Nanoparticles and Their Application in Magneto-Immunosandwich Assay. *Adv. Funct. Mater.* **2016,** 26, 4094-4098.

(15) Mayorga-Martinez, C. C.; Mohamad Latiff, N.; Eng, A. Y. S.; Sofer, Z.; Pumera, M., Black Phosphorus Nanoparticle Labels for Immunoassays via Hydrogen Evolution Reaction Mediation. *Anal. Chem.* **2016,** 88, 10074-10079.

(16) Gusmão, R.; Sofer, Z.; Pumera, M., Black Phosphorus Rediscovered: From Bulk Material to Monolayers. *Angew. Chem. Int. Ed.* **2017,** 56, 8052-8072.

(17) Ares, P.; Palacios, J. J.; Abellan, G.; Gomez-Herrero, J.; Zamora, F., Recent Progress on Antimonene: A New Bidimensional Material. *Adv. Mater.* **2018,** 30, 1703771.

(18) Miotke, L.; Maity, A.; Ji, H.; Brewer, J.; Astakhova, K., Enzyme-Free Detection of Mutations in Cancer DNA Using Synthetic Oligonucleotide Probes and Fluorescence Microscopy. *PLoS One* **2015,** 10, e0136720.

(19) Taskova, M.; Madsen, C. S.; Jensen, K. J.; Hansen, L. H.; Vester, B.; Astakhova, K., Antisense Oligonucleotides Internally Labeled with Peptides Show Improved Target Recognition and Stability to Enzymatic Degradation. *Bioconj. Chem.* **2017,** 28, 768-774.

(20) Choi, Y.; Schmidt, C.; Tinnefeld, P.; Bald, I.; Rödiger, S., A new reporter design based on DNA origami nanostructures for quantification of short oligonucleotides using microbeads. *Sci. Rep.* **2019,** 9, 4769.

(21) Dahan, L.; Huang, L.; Kedmi, R.; Behlke, M. A.; Peer, D., SNP Detection in mRNA in Living Cells Using Allele Specific FRET Probes. *PLoS One* **2013,** 8, e72389.

(22) Mao, F.; Wen, L.; Sun, C.; Zhang, S.; Wang, G.; Zeng, J.; Wang, Y.; Ma, J.; Gao, M.; Li, Z., Ultrasmall Biocompatible Bi2Se3 Nanodots for Multimodal Imaging-Guided Synergistic Radiophotothermal Therapy against Cancer. *ACS Nano* **2016,** 10, 11145-11155.

(23) Zhang, S.; Sun, C.; Zeng, J.; Sun, Q.; Wang, G.; Wang, Y.; Wu, Y.; Dou, S.; Gao, M.; Li, Z., Ambient Aqueous Synthesis of Ultrasmall PEGylated Cu2−xSe Nanoparticles

as a Multifunctional Theranostic Agent for Multimodal Imaging Guided Photothermal Therapy of Cancer. *Adv. Mater.* **2016,** 28, 8927-8936.

(24) Sun, C.; Wen, L.; Zeng, J.; Wang, Y.; Sun, Q.; Deng, L.; Zhao, C.; Li, Z., One-pot solventless preparation of PEGylated black phosphorus nanoparticles for photoacoustic imaging and photothermal therapy of cancer. *Biomaterials* **2016,** 91, 81-89.

(25) Martinez-Perinan, E.; Down, M. P.; Gibaja, C.; Lorenzo, E.; Zamora, F.; Banks, C. E., Antimonene: A Novel 2D Nanomaterial for Supercapacitor Applications. *Adv. Energ. Mater.* **2018,** 8, 1702606.

(26) Hajian, R.; Tavakol, M., Interaction of Anticancer Drug Methotrexate with DS-DNA Analyzed by Spectroscopic and Electrochemical Methods. *J. Chem.* **2012,** 9, 471-480.

(27) Saha, I.; Hossain, M.; Kumar, G. S., Base pair specificity and energetics of binding of the phenazinium molecules phenosafranine and safranine-O to deoxyribonucleic acids: a comparative study. *Phys. Chem. Chem. Phys.* **2010,** 12, 12771-12779.

(28) Zhang, L. Z.; Tang, G.-Q., The binding properties of photosensitizer methylene blue to herring sperm DNA: a spectroscopic study. *J. Photochem. Photobiol. B Biol.* **2004,** 74, 119-125.

(29) Palecek, E.; Fojta, M.; Tomschik, M.; Wang, J., Electrochemical biosensors for DNA hybridization and DNA damage. *Biosens. Bioelectron.* **1998,** 13, 621-628.

(30) Wang, J., Electrochemical biosensors: Towards point-of-care cancer diagnostics. *Biosens. Bioelectron.* **2006,** 21, 1887-1892.

(31) Wan, Y.; Zhang, J.; Liu, G.; Pan, D.; Wang, L. H.; Song, S. P.; Fan, C. H., Ligase-based multiple DNA analysis by using an electrochemical sensor array. *Biosens. Bioelectron.* **2009,** 24, 1209-1212.

(32) Marmur, J., A procedure for the isolation of deoxyribonucleic acid from micro-organisms. *J. Mol. Biol.* **1961,** 3, 208-218.

(33) Doty, P.; Rice, S. A., The denaturation of desoxypentose nucleic acid. *Biochim. Biophys. Acta* **1955,** 16, 446-448.

(34) Meehan, T.; Gamper, H.; Becker, J. F., Characterization of reversible, physical binding of benzo[a]pyrene derivatives to DNA. *J. Biol. Chem.* **1982,** 257, 10479-10485.

(35) Trasatti, S.; Petrii, O. A., Real Surface Area Measuraments in Electrochemistry. *Pure Appl. Chem.* **1991,** 63, 711-734.

(36) Becke, A. D., Density-functional exchange-energy approximation with correct asymptotic behavior. *Phys. Rev. A* **1988,** 38, 3098-3100.

(37) Lee, C.; Yang, W.; Parr, R. G., Development of the Colle-Salvetti correlation-energy formula into a functional of the electron density. *Phys. Rev. B* **1988,** 37, 785-789.

(38) Wadt, W. R.; Hay, P. J., Ab initio effective core potentials for molecular calculations. Potentials for main group elements Na to Bi. *J. Chem. Phys.* **1985,** 82, 284-298.

(39) Palacios, J. J.; Pérez-Jiménez, A. J.; Louis, E.; SanFabián, E.; Vergés, J. A., First-principles approach to electrical transport in atomic-scale nanostructures. *Phys. Rev. B* **2002,** 66, 035322.

(40) Jacob, D.; Palacios, J. J., Critical comparison of electrode models in density functional theory based quantum transport calculations. *J. Chem. Phys.* **2011,** 134, 044118.

For Table of Contents Only